LETTER

doi:10.1038/nature11031

Thermal and electrical conductivity of iron at Earth's core conditions

Monica Pozzo[1], Chris Davies[2], David Gubbins[2,3] & Dario Alfè[1,4]

The Earth acts as a gigantic heat engine driven by the decay of radiogenic isotopes and slow cooling, which gives rise to plate tectonics, volcanoes and mountain building. Another key product is the geomagnetic field, generated in the liquid iron core by a dynamo running on heat released by cooling and freezing (as the solid inner core grows), and on chemical convection (due to light elements expelled from the liquid on freezing). The power supplied to the geodynamo, measured by the heat flux across the core–mantle boundary (CMB), places constraints on Earth's evolution[1]. Estimates of CMB heat flux[2–5] depend on properties of iron mixtures under the extreme pressure and temperature conditions in the core, most critically on the thermal and electrical conductivities. These quantities remain poorly known because of inherent experimental and theoretical difficulties. Here we use density functional theory to compute these conductivities in liquid iron mixtures at core conditions from first principles—unlike previous estimates, which relied on extrapolations. The mixtures of iron, oxygen, sulphur and silicon are taken from earlier work[6] and fit the seismologically determined core density and inner-core boundary density jump[7,8]. We find both conductivities to be two to three times higher than estimates in current use. The changes are so large that core thermal histories and power requirements need to be reassessed. New estimates indicate that the adiabatic heat flux is 15 to 16 terawatts at the CMB, higher than present estimates of CMB heat flux based on mantle convection[1]; the top of the core must be thermally stratified and any convection in the upper core must be driven by chemical convection against the adverse thermal buoyancy or lateral variations in CMB heat flow. Power for the geodynamo is greatly restricted, and future models of mantle evolution will need to incorporate a high CMB heat flux and explain the recent formation of the inner core.

First principles calculations of transport properties based on density functional theory (DFT) have been used in the past for a number of materials (see, for example, refs 9, 10). Recently, increased computer power has facilitated simulations of large systems, allowing the problem of the size of the simulation cell to be addressed: this can be a serious problem for the electrical conductivity, σ (ref. 11). Here we report a series of calculations of the electrical and thermal conductivity (k) of iron at Earth's core conditions, using DFT. We previously used these methods to compute an extensive number of thermodynamic properties of iron and iron alloys, including the whole melting curve of iron in the pressure range 50–400 GPa (refs 12, 13) and the chemical potentials of oxygen, sulphur and silicon in solid and liquid iron at inner core boundary (ICB) conditions, which we used to place constraints on core composition[6]. Recently, we computed the conductivity of iron at ambient conditions, and obtained values in very good agreement with experiments[14].

We calculated three adiabatic temperature–pressure profiles (adiabats) for the core; to do this, we assumed three different possible temperatures at the ICB, and followed the line of constant entropy as the pressure was reduced to that of the CMB. The ICB temperatures were: 6,350 K (the melting temperature of pure iron)[13], 5,700 K (the melting temperature of a mixture of iron with 10% Si and 8% O, corresponding to an inner-core density jump $\Delta\rho = 0.6\,\mathrm{g\,cm^{-3}}$)[6] and 5,500 K (the melting temperature of a mixture of iron with 8% Si and 13% O, corresponding to $\Delta\rho = 0.8\,\mathrm{g\,cm^{-3}}$)[6]. Then we calculated the electrical and thermal conductivity of iron at seven positions on these three adiabats. Our results are reported in Fig. 1, and show a smooth variation of these parameters in the core; σ only varies by ~13% between the ICB and the CMB, and it is almost the same for all adiabats. A recent shock wave experiment[15] reported $\sigma = 0.765 \times 10^6\,\Omega^{-1}\,\mathrm{m}^{-1}$ for pure iron at 208 GPa, and an older shock wave measurement[16] reported $\sigma = 1.48 \times 10^6\,\Omega^{-1}\,\mathrm{m}^{-1}$ at 140 GPa. Our values are closer to the latter. There is a larger variation in k, as implied by the Wiedemann–Franz law (which relates the thermal and electrical conductivity through $L = k/\sigma T$), which we found to be closely followed throughout the core with a Lorenz parameter $L = (2.48–2.5) \times 10^{-8}\,\mathrm{W\,\Omega\,K^{-2}}$. The ionic contribution to k was calculated using the classical potential used as a reference system in ref. 12, which was shown to describe very accurately the energetics of the system and the structural and dynamical properties of liquid iron at Earth's core conditions. We found that the ionic contribution is only between 2.5 and $4\,\mathrm{W\,m^{-1}\,K^{-1}}$ on the adiabat, which is negligible compared to the electronic contribution, as expected.

The estimates of k (Fig. 1) are substantially larger than previously used in the geophysical literature, approximately doubling the heat conducted down the adiabatic gradient in the core and halving the power to drive a dynamo generating the same magnetic field. These considerations demand a revision of the power requirements for the geodynamo. The conductivities for liquid mixtures appropriate to the outer core are likely to be smaller than for pure iron, preliminary calculations suggesting about 30% lower, a smaller difference than that found in previous work[17], but in close agreement with extrapolations obtained from recent diamond-anvil-cell experiments, which reported a value in the range 90–130 $\mathrm{W\,m^{-1}\,K^{-1}}$ at the top of the outer core[18]. Our values are also in broad agreement with recently reported DFT calculations[19].

We focus on estimates for the two mixtures above, corresponding to ICB density jumps $0.6\,\mathrm{g\,cm^{-3}}$ (ref. 8) and $0.8\,\mathrm{g\,cm^{-3}}$ (ref. 7). There is relatively little effect on the conductivities in the two cases, because any additional O in the outer core must be balanced by less S or Si to maintain the mass of the whole core, which is well constrained. The larger density jump gives a higher O content, more gravitational energy, a lower ICB temperature and lower adiabatic gradient: it therefore favours compositional over thermal convection. The relevant values are given in Table 1.

We estimate power requirements for the dynamo using the model described in a previous study (ref. 5, and Methods). Neglecting small effects, the total CMB heat flux, Q_{CMB}, is the sum of terms proportional to either the CMB cooling rate, $\mathrm{d}T_0/\mathrm{d}t$, or the amount of radiogenic heating, h: $Q_{\mathrm{CMB}} = Q_{\mathrm{s}} + Q_{\mathrm{L}} + Q_{\mathrm{g}} + Q_{\mathrm{r}}$, where the terms

[1]Department of Earth Sciences, and Thomas Young Centre at UCL, UCL, Gower Street, London WC1E 6BT, UK. [2]School of Earth and Environment, University of Leeds, Leeds LS2 9JT, UK. [3]Institute of Geophysics and Planetary Physics, Scripps Institution of Oceanography, University of California at San Diego, 9500 Gilman Drive no. 0225, La Jolla, California 92093-0225, USA. [4]Department of Physics and Astronomy, and London Centre for Nanotechnology, UCL, Gower Street, London WC1E 6BT, UK.

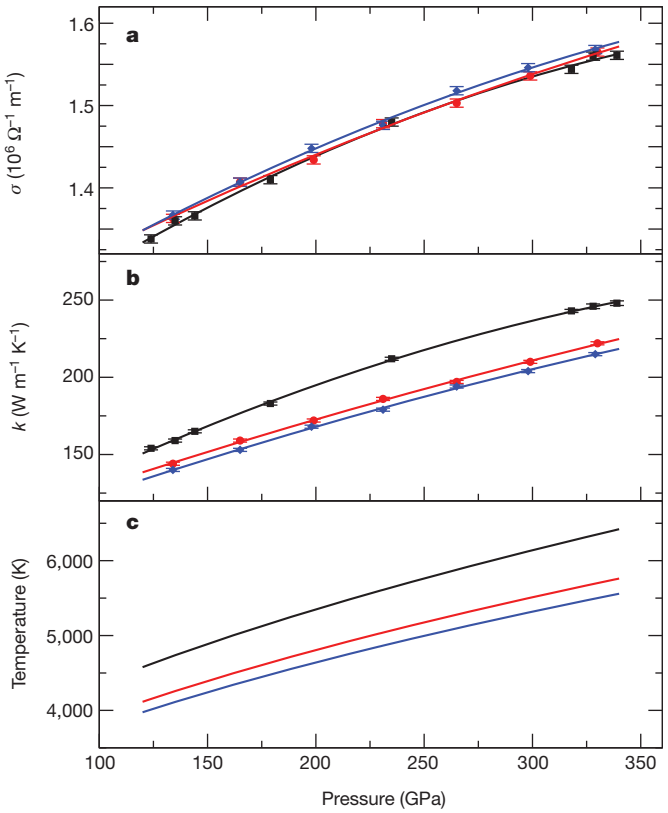

Figure 1 | Electrical and thermal conductivity of iron at Earth's outer core conditions. **a**–**c**, Electrical conductivity, σ (**a**), and electronic component of thermal conductivity, k (**b**), of pure iron corresponding to the three outer-core adiabatic profiles (adiabats) displayed in **c**. Black lines, adiabat corresponding to the melting temperature of pure iron at ICB pressure; red lines, that of the mixture containing 10% Si and 8% O; and blue lines, that of the mixture with 8% Si and 13% O. Lines are quadratic fits to the first principles raw data (symbols). Error bars (2 s.d.) are estimated from the scattering of the data obtained from 40 statistical independent configurations. Results are obtained with cells including 157 atoms and the single **k**-point (1/4,1/4,1/4), which are sufficient to obtain convergence within less than 1%.

on the right-hand side represent respectively the effects of secular cooling, latent heat, gravitational energy and radiogenic heating. The cooling rate, expressed in degrees per billion years, can be varied together with the radiogenic heating to produce some desired outcome: a fixed mantle heat flux, a marginal dynamo (no entropy left for ohmic dissipation, E_σ), or a primordial inner core (by decreasing the cooling rate and increasing the radiogenic heating). Results for a suite of 11 models are shown in Table 2.

Model 1 fails as a dynamo. There is an entropy deficit, meaning the assumption that the whole core can convect is incorrect—the temperature gradient must fall below the adiabat to balance the entropy equation. A dynamo might still be possible with a large part of the core completely stratified. Model 2 demonstrates the efficiency of compositional convection: the entropy is greatly increased compared to model 1 with no change in cooling rate and little increase in heat flux; the dynamo is now marginal. Model 3 has an increased cooling

Table 1 | Parameters used to estimate power requirements for the geodynamo

$\Delta\rho$	T_{ICB}	T_{CMB}	k_{ICB}	k_{CMB}	σ_{ICB} ($\times10^6$)	σ_{CMB} ($\times10^6$)	O	S/Si
0.6	5,700	4,186	150 (223)	100 (144)	1.25 (1.56)	1.11(1.36)	8	10
0.8	5,500	4,039	150 (215)	100 (140)	1.24(1.57)	1.11(1.37)	13	8

Values in parenthesis are for pure iron, other values are approximations for core mixtures. Units are g cm^{-3} for the ICB density jump, $\Delta\rho$; K for the temperatures, T; W m^{-1} K^{-1} for the thermal conductivity, k; Ω^{-1} m^{-1} for the electrical conductivity, σ; % for molar concentrations.

Table 2 | Heat flux and entropy for various models of cooling and radiogenic heating

Model	$\Delta\rho$	dT_O/dt	h	Q_{ad}	Q_{CMB}	IC age	E_σ	Δ
1	0.6	46	0	15.7	5.8	0.9	−111	1,022
2	0.8	46	0	15.2	6.1	1.0	5	826
3	0.6	57	0	15.7	7.2	0.7	−2	833
4	0.6	123	0	15.7	15.6	0.3	652	110
5	0.8	115	0	15.2	15.2	0.4	865	0
6	0.6	46	3.0	15.7	11.7	0.9	85	659
7	0.8	46	3.0	15.2	11.9	1.0	208	468
8	0.6	11.2	6.8	15.7	14.7	3.5	−3	1,257
9	0.6	8.7	6.9	15.7	14.5	4.5	−1	1,472
10	0.8	12.2	6.3	15.2	13.7	3.5	4	1,000
11	0.8	9.5	6.6	15.2	14.1	4.5	2	1,128

Here $\Delta\rho$ is the density jump at the ICB in g cm^{-3}; dT_O/dt the cooling rate of the CMB in K Gyr^{-1}; h the radiogenic heat source in pW kg^{-1}; $Q_{ad} = -4\pi k(dT_{ad}/dr)$ is the heat conducted down the adiabat in TW where dT_{ad}/dr is the adiabatic gradient; Q_{CMB} is the heat flux across the CMB in TW; E_σ is the entropy available for the dynamo and other diffusive processes in MW K^{-1}. Inner core (IC) age is shown in Gyr; stable layer thicknesses, Δ, are given in kilometres below the CMB.

rate and consequent younger inner core to demonstrate what is required for a marginal dynamo with $\Delta\rho = 0.6$ g cm^{-3}. Models 4 and 5 have cooling rates that make the CMB thermally neutral; the CMB heat flux is equal to that conducted down the adiabat. Models 6 and 7 have some radiogenic heating and the original cooling rate and operate as dynamos, although they are still thermally stable at the top of the core. Models 8–11 have cooling rates that yield old inner-core ages, 3.5 and 4.5 Gyr, and the radiogenic heating has been adjusted to make a marginal dynamo. They are also thermally stable at the top of the core.

We estimate stable layer thicknesses by computing the radial variation of thermal and compositional gradients for each model using the equations of a previous study (ref. 20, Methods), which are derived from the equations of core energetics[5]. To compare thermal and chemical gradients, we multiply the latter by the ratio of compositional and thermal expansion coefficients α_c/α_T, thereby converting compositional effects into equivalent thermal effects. The base of the stable layer is defined as the point where the stabilizing adiabatic gradient, T'_a, crosses the combined destabilizing gradient, $T' = T'_L + T'_s + T'_c + T'_r$, where the terms represent respectively latent heat, secular cooling, compositional buoyancy and radiogenic heating.

Stable layer thicknesses are hundreds of kilometres in all models except those with cooling rates that are so rapid as to make the inner core too young; without compositional buoyancy the layers in all models except 4 and 5 span half the core (Table 2). Radiogenic heating thins the layers for the same cooling rate. Profiles of stabilizing and destabilizing gradients (Fig. 2) show that destabilizing gradients are greatest at depth, but much reduced compared to previous models[20] because they each depend on a factor $1/k$. The thermal conductivity increases by 50% across the core, increasing the heat conducted down the adiabat at depth and further reducing the power available to drive convection near the base of the outer core. Combined thermochemical profiles suggest that compositional buoyancy near the top of core is not strong enough to drive convection against the adverse temperature gradient.

Stable layers could be thinned or partially disturbed by convection, through penetration or instability, or some other effect not included in our simple model. A potentially more effective mechanism for inducing vertical mixing near the CMB is through lateral variations in CMB heat flux, which can drive motions without having to overcome the gravitational force. The presence of lateral variations makes the relevant heat flux for core mixing the maximum at the CMB[21], which could be as much as 10 times the average[22]; this does not influence dynamo entropy calculations but does allow magnetic flux to be carried to the surface in regions of cold mantle, as is observed[23].

As well as raising k, our calculations also raise σ to about twice the current estimate. Two important quantities depend on σ: the magnetic diffusion time (the time taken for the slowest decaying dipole mode to fall by a factor of e in the absence of a dynamo) and the magnetic Reynolds number Rm, which measures the rate of generation of

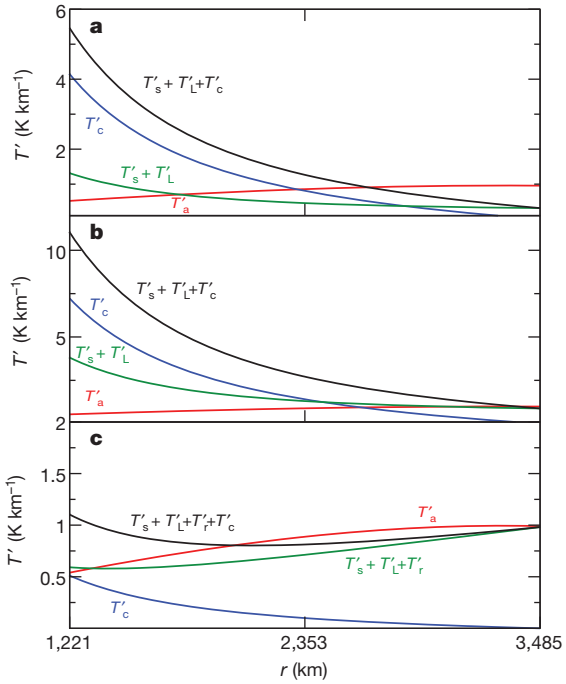

Figure 2 | Stabilizing and destabilizing gradients for three core energetics models. Equivalent temperature gradients, T', plotted against radius for three core evolution models. The stabilizing gradient is due to conduction down the adiabat, T'_a (red lines). Compositional buoyancy is denoted by T'_c (blue lines), latent heat by T'_L, secular cooling by T'_s and radiogenic heating by T'_r. The total destabilizing thermal gradient is represented by the green lines; total destabilizing thermochemical gradients are represented by black lines. Three models from Table 2 are shown: **a**, model 2 ($\Delta\rho = 0.8\,\mathrm{g\,cm^{-3}}$, $dT_o/dt = 46\,\mathrm{K\,Gyr^{-1}}$ and $h = 0$); **b**, model 4 ($\Delta\rho = 0.6\,\mathrm{g\,cm^{-3}}$, $dT_o/dt = 123\,\mathrm{K\,Gyr^{-1}}$ and $h = 0$); **c**, model 9 ($\Delta\rho = 0.6\,\mathrm{g\,cm^{-3}}$, $dT_o/dt = 8.7\,\mathrm{K\,Gyr^{-1}}$ and $h = 6.9\,\mathrm{pW\,kg^{-1}}$).

magnetic energy by a given flow. The magnetic diffusion time is increased to about 50 kyr. This may have significant implications for the theory of the secular variation: it makes the frozen flux approximation more accurate and lengthens the timescale of all diffusion-dominated processes, including polarity reversals. If current estimates of Rm are appropriate for the core[24], the increased conductivity implies that the geodynamo can operate on slower fluid flows and less input power from thermal and compositional convection.

Revised estimates of σ and k calculated directly at core conditions have fundamental consequences for the thermochemical evolution of the deep Earth. New estimates of the power requirements for the geodynamo suggest a CMB heat flux in the upper range of what is considered reasonable for mantle convection unless very marginal dynamo action can be sustained, while a primordial inner core is only possible with a significant concentration of radiogenic elements in the core. There are objections to a high CMB heat flux and also to radiogenic heating in the core[25–27], but one of the two seems inevitable if we are to have a dynamo. If the inner core is young, these high values of conductivity provide further problems with maintaining a purely thermally driven dynamo. A thermally stratified layer at the top of the core also appears inevitable. Viable thermal history models that produce thin stable layers and an inner core of age ~1 Gyr are likely to require a fairly rapid cooling rate and some radiogenic heating. The presence of a stable layer, and the effects associated with an increased electrical conductivity, have significant implications for our understanding of the geomagnetic secular variation.

METHODS SUMMARY

Calculations were performed using DFT with the same technical parameters used in refs 6, 12–14. We used the VASP code[28], PAW potentials[29,30] with $4s^1 3d^7$ valence configuration, the Perdew–Wang[31] functional, a plane wave cut-off of 293 eV, and single particle orbitals were occupied according to Fermi–Dirac statistics. We tested the effect on the conductivity of the inclusion in valence of semi-core 3*s* and 3*p* states; we found that, as in the zero pressure case[14], this effect is completely negligible.

The electrical conductivity and the electrical component of the thermal conductivity have been calculated using the Kubo–Greenwood formula and the Chester–Thellung–Kubo–Greenwood formula as implemented in VASP[32]. Because of the low mass of the electrons compared to the ions, the conductivities may be calculated by assuming frozen ionic configurations, and averaging over a sufficiently large set representing the typical distribution of the ions at the pressures and temperatures of interest.

Molecular dynamics simulations were performed in the canonical ensemble using cubic simulation cells with 157 atoms and the Γ point, a time step of 1 fs, and an efficient extrapolation of the charge density which speeds up the simulations by roughly a factor of two (ref. 33). Each state point was simulated for at least 6 ps, from which we discarded the first picosecond to allow for equilibration and used the last 5 ps to extract 40 configurations separated by 0.125 ps. This time interval is roughly two times longer than the correlation time, and therefore the configurations are statistically independent from each other. Because of the high temperatures involved, the conductivities converge quickly with respect to **k**-point sampling and size of the simulation cell[14], and we found that with a 157-atom cells and the single **k**-point (1/4,1/4/,1/4) the results are converged to better than 1%.

The ionic component of the thermal conductivity was calculated using the Green–Kubo formula.

Full Methods and any associated references are available in the online version of the paper at www.nature.com/nature.

Received 23 November 2011; accepted 7 March 2012.
Published online 11 April 2012.

1. Lay, T., Hernlund, J. & Buffett, B. Core-mantle boundary heat flow. *Nature Geosci.* **1,** 25–32 (2008).
2. Labrosse, S., Poirier, J.-P. & Le Mouël, J.-L. On cooling of the Earth's core. *Phys. Earth Planet. Inter.* **99,** 1–17 (1997).
3. Buffett, B., Garnero, E. & Jeanloz, R. Sediments at the top of Earth's core. *Science* **290,** 1338–1342 (2000).
4. Lister, J. R. & Buffett, B. A. The strength and efficiency of thermal and compositional convection in the geodynamo. *Phys. Earth Planet. Inter.* **91,** 17–30 (1995).
5. Gubbins, D., Alfè, D., Masters, T. G. & Price, D. Gross thermodynamics of 2-component core convection. *Geophys. J. Int.* **157,** 1407–1414 (2004).
6. Alfè, D., Gillan, M. J. & Price, G. D. Temperature and composition of the Earth's core. *Contemp. Phys.* **48,** 63–80 (2007).
7. Masters, T. G. & Gubbins, D. On the resolution of density within the Earth. *Phys. Earth Planet. Inter.* **140,** 159–167 (2003).
8. Dziewonski, A. M. & Anderson, D. L. Preliminary Reference Earth Model. *Phys. Earth Planet. Inter.* **25,** 297–356 (1981).
9. Silvestrelli, P. L., Alavi, A. & Parrinello, M. Electrical conductivity calculation in ab initio simulations of metals: application to liquid sodium. *Phys. Rev. B* **55,** 15515–15522 (1997).
10. Mattsson, T. R. & Desjarlais, M. P. Phase diagram and electrical conductivity of high energy density water from density functional theory. *Phys. Rev. Lett.* **97,** 017801 (2007).
11. Pozzo, M., Desjarlais, M. P. & Alfè, D. Electrical and thermal conductivity of liquid sodium from first principles calculations. *Phys. Rev. B* **84,** 054203 (2011).
12. Alfè, D., Gillan, M. J. & Price, G. D. The melting curve of iron at the pressures of the Earth's core conditions. *Nature* **401,** 462–464 (1999).
13. Alfè, D. Temperature of the inner-core boundary of the Earth: melting of iron at high pressure from first-principles coexistence simulations. *Phys. Rev. B* **79,** 060101(R) (2009).
14. Alfè, D., Pozzo, M. & Desjarlais, M. P. Lattice electrical resistivity of magnetic body-centred cubic iron from first principles calculations. *Phys. Rev. B* **85,** 024102 (2012).
15. Bi, Y., Tan, H. & Jing, F. Electrical conductivity of iron under shock compression up to 200 GPa. *J. Phys. Condens. Matter* **14,** 10849–10854 (2002).
16. Keeler, R. N. & Royce, E. B. in *Physics of High Energy Density* (eds Caldirola, P. & Knoepfel, H.) 106–125 (Proc. Int. Sch. Phys. Enrico Fermi Vol. 48, 1971).
17. Stacey, F. D. & Anderson, O. L. Electrical and thermal conductivities of Fe–Ni–Si alloy under core conditions. *Phys. Earth Planet. Inter.* **124,** 153–162 (2001).
18. Hirose, K. Gomi, H. Ohta, K., Labrosse, S. & Hernlund, J. The high conductivity of iron and thermal evolution of the Earth's core. *Mineral. Mag.* **75,** 1027 (2011).
19. de Koker, N., Steinle-Neumann, G. & Vlcek, V. Electrical resistivity and thermal conductivity of liquid Fe alloys at high P and T, and heat flux in Earth's core. *Proc. Natl Acad. Sci.* **109,** 4070–4073 (2012).
20. Davies, C. J. & Gubbins, D. A buoyancy profile for the Earth's core. *Geophys. J. Int.* **187,** 549–563 (2011).
21. Olson, P. in *Earth's Core and Lower Mantle* (eds Jones, C., Soward, A. & Zhang, K.) 1–49 (Taylor and Francis, London, 2000).

22. Nakagawa, T., &. Tackley, P. J. Lateral variations in CMB heat flux and deep mantle seismic velocity caused by a thermal-chemical-phase boundary layer in 3D spherical convection. *Earth Planet. Sci. Lett.* **271,** 348–358 (2008).
23. Jackson, A., Jonkers, A. R. T. & Walker, M. R. Four centuries of geomagnetic secular variation from historical records. *Phil. Trans. R. Soc. Lond. B* **358,** 957–990 (2000).
24. Gubbins, D. in *Encyclopedia of Geomagnetism and Paleomagnetism* (eds Gubbins, D. & Herrero-Bervera, E.) 287–300 (Springer, 2007).
25. Davies, G. Topography: a robust constraint on mantle fluxes. *Chem. Geol.* **145,** 479–489 (1998).
26. Davies, G. Mantle regulation of core cooling: a geodynamo without core radioactivity? *Phys. Earth Planet. Inter.* **160,** 215–229 (2007).
27. McDonough, W. in *Treatise on Geochemistry* Vol. 2 (ed. Carlson, R. W.) 547–568 (Elsevier, 2003).
28. Kresse, G. & Furthmuller, J. Efficiency of ab-initio total energy calculations for metals and semiconductors using a plane-wave basis set. *Comput. Mater. Sci.* **6,** 15–50 (1996).
29. Blöchl, P. E. Projector augmented-wave method. *Phys. Rev. B* **50,** 17953–17979 (1994).
30. Kresse, G&. Joubert, D. From ultrasoft pseudopotentials to the projector augmented-wave method. *Phys. Rev. B* **59,** 1758–1775 (1999).
31. Wang, Y. & Perdew, J. P. Correlation hole of the spin-polarized electron gas, with exact small-wave-vector and high-density scaling. *Phys. Rev. B* **44,** 13298–13307 (1991).
32. Desjarlais, M. P., Kress, J. D. & Collins, L. A. Electrical conductivity for warm, dense aluminum plasmas and liquids. *Phys. Rev. E* **66,** 025401(R) (2002).
33. Alfè, D. Ab initio molecular dynamics, a simple algorithm for charge extrapolation. *Comput. Phys. Commun.* **118,** 31–33 (1999).

Supplementary Information is linked to the online version of the paper at www.nature.com/nature.

Acknowledgements D.G. is supported by CSEDI grant EAR1065597 from the National Science Foundation. C.D. is supported by a Natural Environment Research Council personal fellowship, NE/H01571X/1. M.P. is supported by NERC grant NE/H02462X/1 to D.A. Calculations were performed on the UK national facility HECToR.

Author Contributions D.A. and D.G. designed the project. M.P. and D.A. performed the first principles calculations. C.D. and D.G. performed the thermal history and core stratification calculations. All authors discussed the results and commented on the manuscript.

Author Information Reprints and permissions information is available at www.nature.com/reprints. The authors declare no competing financial interests. Readers are welcome to comment on the online version of this article at www.nature.com/nature. Correspondence and requests for materials should be addressed to D.A. (d.alfe@ucl.ac.uk).

METHODS

First principles calculations. Calculations were performed using DFT with the same technical parameters used in refs 6, 12–14. We used the VASP code[28], PAW potentials[29,30] with $4s^1 3d^7$ valence configuration, the Perdew–Wang[31] functional, a plane wave cut-off of 293 eV, and single particle orbitals were occupied according to Fermi–Dirac statistics. We tested the effect on the conductivity of the inclusion in valence of semi-core 3*s* and 3*p* states; we found that, as in the zero pressure case[14], this effect is completely negligible.

The electrical conductivity and the electrical component of the thermal conductivity have been calculated using the Kubo–Greenwood formula and the Chester–Thellung–Kubo–Greenwood formula as implemented in VASP[32]. Because of the low mass of the electrons compared to the ions, the conductivities may be calculated by assuming frozen ionic configurations, and averaging over a sufficiently large set representing the typical distribution of the ions at the pressures and temperatures of interest.

Molecular dynamics simulations were performed in the canonical ensemble using cubic simulation cells with 157 atoms and the Γ point, a time step of 1 fs, and an efficient extrapolation of the charge density which speeds up the simulations by roughly a factor of two (ref. 33). Each state point was simulated for at least 6 ps, from which we discarded the first picosecond to allow for equilibration and used the last 5 ps to extract 40 configurations separated by 0.125 ps. This time interval is roughly two times longer than the correlation time, and therefore the configurations are statistically independent from each other. Because of the high temperatures involved, the conductivities converge quickly with respect to **k**-point sampling and size of the simulation cell[14], and we found that with a 157-atom cells and the single **k**-point (1/4,1/4/,1/4) the results are converged to better than 1%.

The ionic component of the thermal conductivity was calculated using the Green–Kubo formula.

Power estimates for the geodynamo. Estimates of the power required to drive the geodynamo are obtained by considering the slow evolution of the Earth using equations describing the balances of energy and entropy in the core. A detailed derivation of these equations can be found in a previous study[5]. Conservation of energy simply equates the heat crossing the CMB to the sources within: specific heat of cooling Q_s, latent heat of freezing Q_L, radiogenic heating Q_r, gravitational energy loss Q_g that is converted into heat by the frictional processes associated with the convection (almost entirely magnetic), and smaller terms[5] involving pressure changes and chemistry that we shall ignore:

$$Q_{CMB} = Q_s + Q_L + Q_g + Q_r \quad (1)$$

All terms on the right-hand side of equation (1) can be written in terms of either the cooling rate at the CMB, dT_0/dt, or the amount of radiogenic heating, h. There is no dependence on the conductivities or the magnetic field, which are merely agents by which energy is converted to heat within the core.

These quantities do enter the entropy balance, however. This equation has dissipation terms from thermal and electrical conduction, plus viscosity and molecular diffusion. They are all positive because of the second law of thermodynamics. They are balanced by entropies associated with the power driving the convection: heat pumped in at a higher temperature and removed at a lower temperature (T_{CMB}) and gravitational energy that directly stirs the core and is converted to heat by frictional processes, the heat then being convected and conducted away. Note that entropy from heat is multiplied by a Carnot-like 'efficiency factor', $1/T_{out} - 1/T_{in}$ (latent heat is the most efficient because it is released at the highest temperature and removed at the lowest), while the gravitational energy is not, $E_g = Q_g/T_{ICB}$. Gravitational energy is more efficient at removing entropy and therefore more efficient than heat at generating magnetic field.

$$E = E_s + E_L + E_r + E_g = E_k + E_\sigma + E_\alpha \quad (2)$$

where the four terms on the left-hand side of the second equality represent secular cooling, latent heat release, radiogenic heating and gravitational energy loss. Adiabatic conduction entropy, E_k, is easily estimated from the thermal conductivity and adiabatic gradient and is large, of order $10^8\,W\,K^{-1}$. The new estimate of conductivity doubles older ones and the higher ICB temperatures increase it still further. Barodiffusion, E_α, is the tendency for light elements to migrate down a pressure gradient and its associated entropy is significant but small, not exceeding $2.5\,MW\,K^{-1}$ in any of our estimates. Diffusional processes associated with convection and the geodynamo also produce entropy, denoted E_σ, mainly in the small scales. This presents a problem in estimation because the dominant contribution comes from magnetic fields, fluid flows, temperature and compositional fluctuations that cannot be observed and, in many cases, cannot even be simulated numerically. A low value of the power required to drive the dynamo, 0.5 TW (ref. 34), was obtained from a numerical dynamo simulation[35], which at an average temperature of 5,000 K translates into $E_\sigma = 10^7\,W\,K^{-1}$, an order of magnitude lower than E_k, but the numerical simulation necessarily reduces small scale magnetic fields and the value for the Earth could be much larger. It may well be that future numerical simulations with higher resolution will have higher ohmic dissipation approaching E_k. Magnetic diffusivity is much larger than any other diffusivity in the core, by many orders of magnitude, and in numerical simulations the viscosity, thermal, and molecular diffusivities are replaced with turbulent values to account for unresolved, turbulent, small scale fields. Even so, the associated entropies remain much smaller than those associated with magnetic fields: they are generally ignored, although we should bear in mind that they are all positive and could make a contribution.

Parameter values used to calculate thermal contributions to the energy and entropy balances equations (1) and (2) are taken from Table 1 of a previous study[36], except for the thermal conductivity and the temperatures of the CMB and ICB, which are taken from the present study. Latent heat, Q_L, depends on τ, the difference between the melting and adiabatic gradients at the ICB; the value for the former is taken to be $9\,K\,GPa^{-1}$ (ref. 36), while the value of the latter is calculated from Fig. 1 of this study. Parameter values used to calculate compositional terms differ slightly from previous work[5], owing to their use of different concentrations for the light elements O, Si and S in the outer core. Concentration enters the calculation of gravitational energy through equation (9) of ref. 5, which, along with equation (8) of ref. 5, is used to define Q_g in equation (18) of ref. 5. Note also Q_g depends on τ. The remaining changes affect the barodiffusion, E_α, which makes a small contribution to the entropy budget (2); for completeness we list the new parameter values required to determine E_α in Supplementary Tables 1 and 2.

Estimating stable layer thicknesses. Radial profiles of the thermal and compositional energy sources that power the dynamo are determined using the equations of a previous study[20], which are derived from the energy balance appropriate for the outer core[5]. The radial profiles represent conductive solutions that satisfy the total CMB heat-flux boundary condition for the temperature, zero CMB mass flux of light elements, and fixed temperature and light element concentration at the ICB[20]. Superimposed on this basic state are the small fluctuations associated with core convection and the dynamo process.

These radial profiles apply to a Boussinesq fluid and hence neglect compressibility effects other than when they act to modify gravity. This necessitates the use of an approximate form for the adiabatic temperature, a simple choice being a quadratic equation expressed in terms of the ICB and CMB temperatures[19]. Despite these simplifications, the CMB heat fluxes computed from equations (23)–(27) of the incompressible model[20] are in good agreement with those obtained from the original equations[5] (see Supplementary Table 3), while the quadratic approximation for the adiabat differs by at most 10 K from the full calculation shown in Fig. 1.

Compositional buoyancy is at least as important for driving the geodynamo as thermal buoyancy (see, for example, ref. 5) and so we require a means of comparing the two in radial profiles, which is readily achieved by multiplying the former by the ratio of compositional and thermal expansion coefficients, α_c/α_T. This simple device converts compositional effects into equivalent thermal effects, thereby allowing all sources of buoyancy to be combined; it is also related to the condition of neutral stability discussed below. (However, it must be understood that the compositional term resulting from this transformation has nothing to do with the gravitational energy, Q_g, which is neglected in the Boussinesq equations[37].) We use the common approach (see, for example, ref. 37) of defining all fluxes that represent sources of buoyancy associated with the convection in terms of a turbulent diffusivity, which is assumed constant. By contrast, the heat flux due to conduction down the adiabatic gradient and the equivalent thermal flux due to barodiffusion must be defined in terms of molecular quantities.

The depth variation of the molecular thermal conductivity obtained from the DFT results is readily incorporated into the formulation of previous work[20]. We write $k = k(r)$ to express the radial variation of the molecular thermal conductivity; equation (8) from ref. 20 must then be replaced by $q_a = \nabla\cdot(k(r)\nabla T_a)$, where ∇T_a is calculated from equation (12) in ref. 20. $k(r)$ is well-approximated by a parabolic conductivity variation, $k(r) = ar^2 + br + c$, which we use to calculate the heat flux down the adiabatic gradient.

To investigate the presence of a stable layer, we use temperature gradients instead of heat fluxes, which are calculated using equations (30)–(34) of a previous study[20] with $k(r)$ replacing k in the numerator of equation (30) of ref. 20. The parameter values are the same as those used to estimate power requirements above. We define the base of the stable layer to be the point of neutral stability as given by Schwarzchild's criterion[38]:

$$\left(\frac{\mathrm{d}T}{\mathrm{d}r}-\frac{\mathrm{d}T_{\mathrm{a}}}{\mathrm{d}r}\right)+\frac{\alpha_{\mathrm{c}}}{\alpha_{\mathrm{T}}}\left(\frac{\mathrm{d}c}{\mathrm{d}r}\right)=0$$

where $\mathrm{d}T/\mathrm{d}r$ is the total temperature gradient, $\mathrm{d}T_{\mathrm{a}}/\mathrm{d}r$ is the adiabatic temperature gradient and $\mathrm{d}c/\mathrm{d}r$ is the total compositional gradient. We write this condition as $T'=T'_{\mathrm{L}}+T'_{\mathrm{s}}+T'_{\mathrm{c}}+T'_{\mathrm{r}}-T'_{\mathrm{a}}=0$, where the terms represent respectively latent heat, secular cooling, compositional buoyancy, radiogenic heating and the adiabat, and prime indicates differentiation with respect to r (the barodiffusive contribution to $\mathrm{d}c/\mathrm{d}r$ is very small and has been omitted). Possible deviations from the layer thicknesses we obtain using this definition can only be obtained by solving the complete dynamo equations with correct parameters for the Earth, which is impossible at present. We believe this to be the best definition of the base of the layer given the nature of our thermodynamic model.

34. Buffett, B. A. Estimates of heat flow in the deep mantle based on the power requirements for the geodynamo. *Geophys. Res. Lett.* **29,** 1566–1569 (2002).
35. Kuang, W. & Bloxham, J. An Earth-like numerical dynamo model. *Nature* **389,** 371–374 (1997).
36. Gubbins, D., Alfè, D., Masters, T. G., Price, D. & Gillan, M. J. Can the Earth's dynamo run on heat alone? *Geophys. J. Int.* **155,** 609–622 (2003).
37. Anufriev, A. P., Jones, C. A. & Soward, A. M. The Boussinesq and anelastic liquid approximations for convection in the Earth's core. *Phys. Earth Planet. Inter.* **152,** 163–190 (2005).
38. Gubbins, D. & Roberts, P. H. in *Geomagnetism* (ed. Jacobs, J. A.) 30–32 (Academic, 1987).